Polypropylene Nanocomposite Using Maleated PP and Diamine

Kwang Hoi Ku, Sung Chul Kim

Department of Chemical and Biomolecular Engineering, Korea Advanced Institute of Science and Technology, Guseong-dong, Yuseong-gu, Daejeon 305-701, Korea

Received 30 April 2008; accepted 11 January 2009
DOI 10.1002/app.30028
Published online 14 April 2009 in Wiley InterScience (www.interscience.wiley.com).

ABSTRACT: The insertion of the aliphatic diamine inside the organoclay will help the dispersion of the clay platelets in the PP/clay nanocomposite due to the reaction between the maleated PP and the diamine. Cloisite®20A was just simply mixed with hexamethylene diamine (HMDA) under shearing condition in Brabender mixer. HMDA group was successfully penetrated into silicate layers. As a result of penetration, d-spacing of organoclay was increased. Polypropylene/clay nanocomposites were prepared by compounding with maleated PP and amine-treated clay. From the FTIR spectra, reaction between amine group and maleic-anhydride group was confirmed. The effect of the organoclay on the properties of the nanocomposite such as the morphology, dynamic mechanical properties, crystal structure and crystallization behavior, glass transition temperature, thermal stability, and tensile properties were investigated and analyzed. Nanocomposites with amine-treated clays show enhanced properties compared with those with non–amine-treated clay (Cloisite®20A). From the TEM analysis, nanocomposites with amine-treated clays shows better dispersibility compared with those with Cloisite®20A alone. © 2009 Wiley Periodicals, Inc. J Appl Polym Sci 113: 1539–1549, 2009

Key words: polypropylene; maleated PP; HMDA; diamine

INTRODUCTION

PP exhibits an attractive combination of low cost, light weight, and good thermal stability, toughness, and recyclability. To improve PPs competitiveness with the engineering plastics, it needs high dimensional stability, stiffness, strength, and impact resistance. Therefore, a special emphasis has been placed on the development of nano-filled PP by means of inorganic or organic nanocomposites.[1–4]

There are many kinds of silicates; hectorite, saponite, montmollironite etc. the layer thickness is around 1 nm, and lateral dimension of these layers may vary from 30 nm to several microns depending on the particular silicate layers. Among them, montmollironite is the most commonly used. In natural state, montmorillonite crystal lattice consists of 1 nm thin layers, with a central octahedral sheet containing alumina or magnesium hydroxide sandwiched by two tetrahedral sheets. Because of the high aspect ratio, clay has an extremely high surface area in delaminated state.

To make enhanced properties in composite materials, it is essential that platelets have high surface area, high aspect ratio, and good wetting characteristics between matrix and inorganic materials. Therefore, disordered, exfoliated silicate layers in a polymer matrix can help to increase their mechanical properties.[5,6]

Recent studies on PP/clay nanocomposites have focused on the uniform dispersion of modified clay platelets in the nonpolar matrix to maximize their physical and mechanical properties.[7–10]

Attempts to fully exfoliate clay platelets in the PP have met many challenges because of the mismatch in surface polarities between clay and PP. In the natural state, the clay is hydrophilic whereas PP is hydrophobic. To render the clay hydrophobic, the aliphatic amine is inserted into the silicate layers as an organifier by means of cation-exchange reaction so that it can improve the compatibility between matrix and silicate layers and increase the interlayer spacing.[11]

In the case of PP, the alkyl ammonium-based silicate layers does not have enough ability to promote PP clay dispersion. So to improve the interactions between polymer and silicate layers, the compatibilizer must be used. Generally, the functionalized PP has been used as a compatibilizer,[12] and PP-g-MA is the most widely used functionalized PP.

In this study, Polybond3200 is also used as a compatibilizer. And this maleated PP has a functional group of maleic anhydirde, which has a high reactivity. It can react with the amine group easily.[13] In

Correspondence to: S. C. Kim (kimsc@kaist.ac.kr).

TABLE I
Composition of Nanocomposites

	Sample Code	PP (wt %)	Polybond 3200 (wt %)	Clay[amine*]	Amine/anhydride mole ratio
Nonequimolar (amine insertion)	B-01	80	18	2[14%]	2.7
	B-02	80	16	4[14%]	6.0
	B-03	80	14	6[14%]	10.4
Nonequimolar (free of amine)	RB-01	80	18.3	1.7[0%]	—
	RB-02	80	16.6	3.4[0%]	—
	RB-03	80	14.9	5.1[0%]	—
Equimolar (amine insertion)	A-01	77.6	20.7	1.7[7%]	1.0
	A-02	55.2	41.4	3.4[7%]	1.0
	A-03	32.8	62.1	5.1[7%]	1.0
Equimolar (free of amine)	RA-01	77.6	20.8	1.6[0%]	—
	RA-02	55.2	41.6	3.2[0%]	—
	RA-03	32.8	62.4	4.8[0%]	—

* Amine content in Cloisite 20A.

the case of hexamethylene diamine (HMDA), it has each amine group in both end. When one side of amine group react with MA group on PP-g-MA chain, the other side still has a chance to react. So this HMDA can act as a bridge between two PP-g-MA chains to form long chain branching polymer. This long chain branches usually decrease the viscosity during the mixing process so that the silicate layers can be well dispersed in the matrix which increase mechanical properties. In addition, this process could help d-spacing of silicate layers to increase more. Because the introduction of a long chain branching into the silicate layers, which originate from the reaction between PP-g-MA and HMDA, can increase d-spacing.

The Cloisite®20A was treated with dimaine (HMDA) in the Brabender Mixer to introduce diamine group into the silicate layers. And PP nanoomposites were prepared by this amine-treated clays and Cloisite®20A.

EXPERIMENTAL

Materials

Polypropylene (M_n: 32,000 M_w: 268,000) with broad molecular weight distribution was obtained from Samsung Total. Maleated-PP [Polybond 3200 (M_w: 127,100, MA content: 1 wt %) from Crompton] was used as a intercalating agent.

Cloisite®20A (Southern Clay Products, USA, CEC = 92.6 meq/100 g) was used as the organoclay, where methyl tallow bis-2-hydroxyl quaternary ammonium was the organifier.

The particle size was less than 20 μm. HMDA, which acts as the reactive intercalating agent, was supplied from Aldrich.

Amine-treated clay

A Brabender mixer was used for the preparation of the amine-treated Cloisite®20A. The temperature of the mixer was maintained at 80°C. The rotor speed was maintained at 50 rpm for 1 h. The amine content was ranged from 7 wt % to 14 wt %. The weight percent of each component was measured by thermogravimetric analyzer (TGA).

Polypropylene nanocomposite

In this study, two different types of nanocomposite were prepared. The first one was prepared by having nonequimolar condition between HMDA and MA group of polybond3200. The other was prepared by mixing in equimolar amine/anhydride condition. The composition of prepared sample is shown in Table I. Polypropylene and modified PP (Polybond3200) were blended with amine-treated Cloisite®20A at 180°C in a Brabender mixer 80 rpm rotor speed for 20 min. After drying the mixture at 80°C for 2days, test specimens for mechanical and thermal analysis were prepared by using compression molding under 2000 psi pressure for 10 min after premelting at 180°C.

Characterization

XRD analysis

Wide-angle X-ray diffraction (WAXD) was conducted at ambient temperature using RIGAKU D/MAX-RC diffractometer with CuKαradiation (β = 0.15418 nm) to measure the d-spacing between silicate layers in PP matrix. The d-spacing of the organoclay was calculated by using Brag's law. Each sample was scanned from $2\theta = 1.2°$ to 9° at a scan rate of 2°/min. The small-angle X-ray scattering

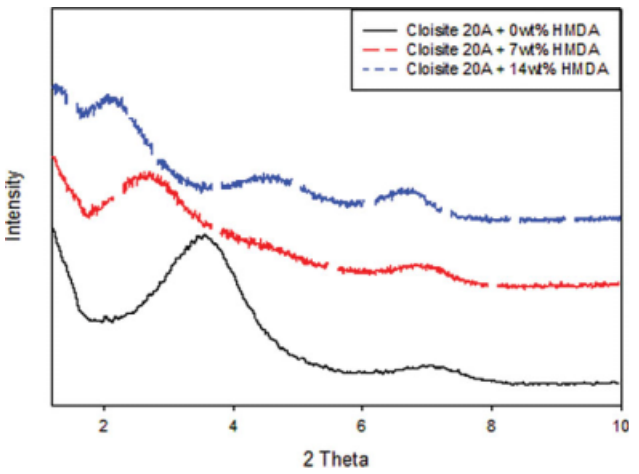

Figure 1 XRD patterns of HMDA-treated clay. [Color figure can be viewed in the online issue, which is available at www.interscience.wiley.com.]

(SAXS) was conducted by using a RIGAKU SWXD in the measurement range from $2\theta = 0.3°$ to 7.0°.

Thermal properties

The thermal properties of the nanocomposites were determined by differential scanning calorimetry (DSC) and TGA.

The melting temperature (T_m), heat of fusion (ΔH_m), crystallization temperature (T_c), heat of crystallization (ΔH_c) of PP nanocomposites were measured by DSC (TA instruments DSC Q100) under nitrogen atmosphere. To eliminate residual crystals that act as a nucleus during cooling process, the sample were maintained at 200°C for 5 min before cooling scan. Cooling scan was conducted from 200°C to 0°C at a rate of 10°C/min, and the heating was conducted from 0°C to 200°C at 10°C/min heating rate.

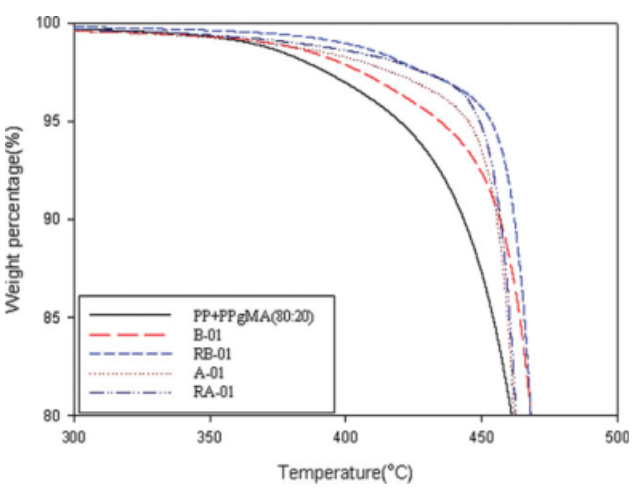

Figure 2 TGA thermogram of nanocomposites. [Color figure can be viewed in the online issue, which is available at www.interscience.wiley.com.]

TABLE II
Inorganic Contents of Nanocomposites

Specimen	Inorganic content (%) 1	2	3
B-x	1.2	1.9	3.2
RB-x	1.0	2.2	3.3
A-x	0.9	1.9	2.8
RA-x	1.0	1.8	3.1

Thermogravimetric analysis was done under nitrogen atmosphere by using a TA Instruments TGA Q500. The measurement was carried out with a heating rate of 20°C/min in the range from 50°C to 650°C.

FTIR analysis

FTIR spectra of the nanocomposites were obtained using JASCO FTIR-470plus. Thin film with thickness of about 100 μm were scanned 50 times with the resolution of 4 cm^{-1}.

Dynamic mechanical analysis

Temperature dependence of dynamic storage modulus was measured by using a Rheometric Scientific dynamic mechanical thermal analyzer (DMTA) IV. DMTA experiments were conducted at 1 Hz frequency with a heating rate of 4°C/min over a temperature range of –80°C to 120°C in dual cantilever mode.

Tensile properties

Tensile test was carried out using an Instron 5583 machine according to ASTM D638 m. The crosshead speed was 50 mm/min.

Morphological analysis

SEM specimens were prepared by etching the nanocomposite surface by O_2 plasma for 7 min. To

TABLE III
TGA Results of Nanocomposites

Properties	Specimen	Inorganic content (%) 0	1	2	3
T_{95} (°C)	B-x	420.1	434.9	445.6	418.8
	RB-x		453.6	448.7	449.9
	A-x	420.1	445.2	439.8	443.9
	RA-x		449.3	450.4	441.9

T_{95}: Temperature at 5 wt % decomposition.

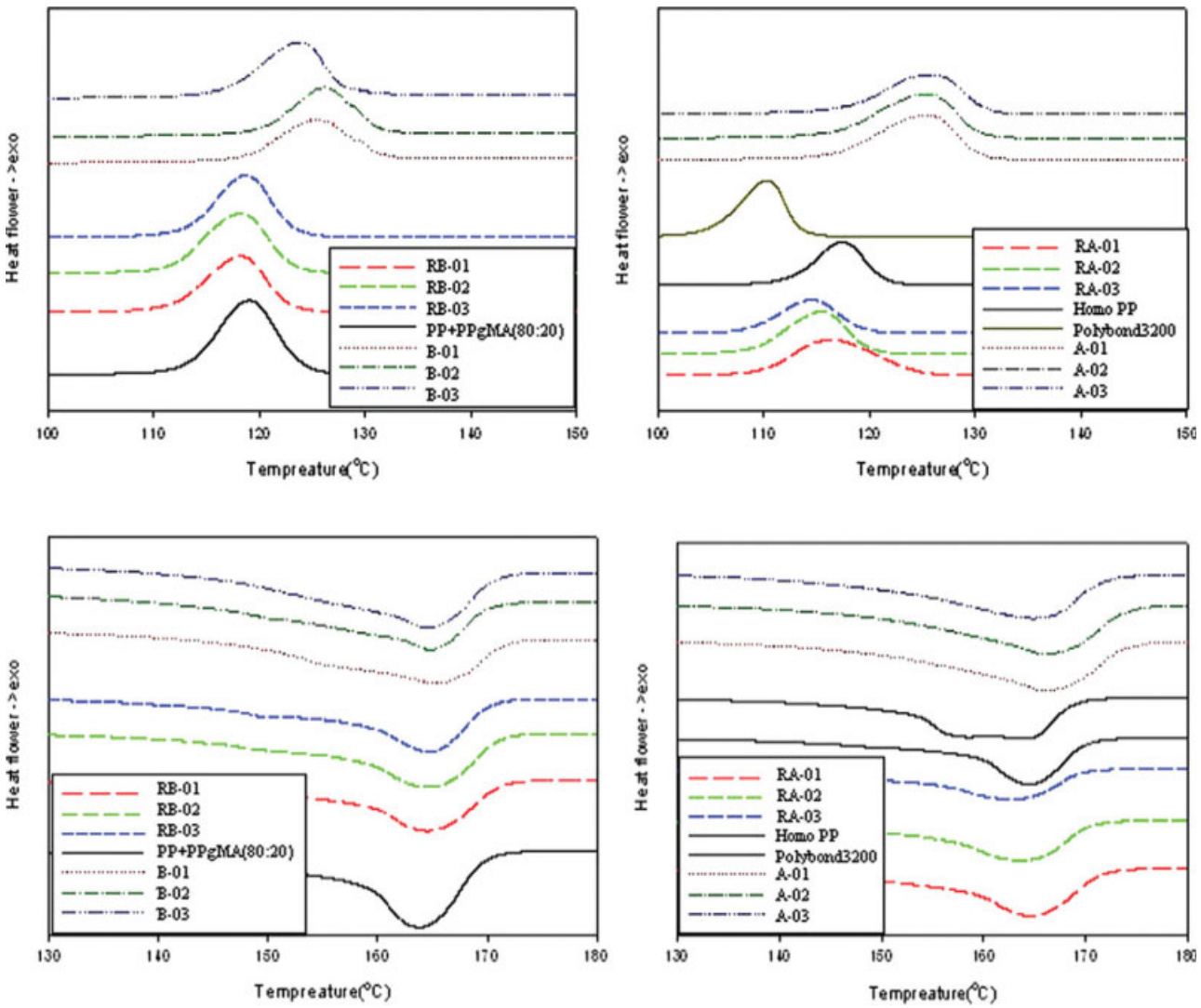

Figure 3 DSC thermogram of nanocomposite (a) cooling scan thermograms of nonequimolar samples, (b) those of equimolar ones, (c) heating scan thermograms of nonequimolar samples, and (d) those of equimolar ones. [Color figure can be viewed in the online issue, which is available at www.interscience.wiley.com.]

observe the residual clay particles, the surface of the plasma-etched nanocomposite was investigated by using Jeol JSM-5610 SEM after gold coating. The specimens for TEM observation were prepared by using a RMC MT-XL microtome with cryogenic CR-XL system. The specimens were cut with a diamond knife at –80°C in the thickness of about 30 nm. TEM micrographs were obtained by using a PHILLIPS CM20 transmission electron microscopy.

RESULTS AND DISCUSSIONS

Figure 1 shows the XRD patterns of Cloisite®20A and amine-treated Cloisite®20A. The Cloisite®20A shows the basal spacing at $2\theta = 3.46^{o}$ corresponding to $d = 2.52$ nm. When Cloisite®20A was treated with HMDA, the peak of basal spacing appeared at lower angle. With an insertion of HMDA, the silicate layer d-spacing was expanded. The basal spacing of 7 wt % and 14 wt % amine-treated clay was 3.37 nm

TABLE IV
DSC Results of Nonequimolar Nanocomposite

Properties	Specimen	Clay content (%)			
		0[a]	1	2	3
T_m (°C)	B-x	163.9	165.6	165.2	164.7
	RB-x		163.8	164.6	164.7
ΔH_m	B-x	93.2	113.6	108.4	101.5
	RB-x		96.5	93.4	90.2
Crystallinity (%)	B-x	56.4	68.8	65.7	61.5
	RB-x		58.5	56.6	54.7
ΔH_c (J/g)	B-x	85.2	116.7	113.4	108.5
	RB-x		111.2	106.3	104.2
T_c (°C)	B-x	118.9	126.8	127.2	124.6
	RB-x		118.2	118.3	118.8

0[a]: PP + Polobond 3200 (80 : 20).

TABLE V
DSC Results of Equimolar Nanocomposite

Properties	Specimen	Clay content (%)			Specimen	
		1	2	3	PP	Polybond3200
T_m (°C)	A-x	166.1	164.7	164.7	164.6	164.2
	RA-x	164.5	163.7	163.1		
ΔH_m	A-x	96.2	93.2	92.9	90.0	80.6
	RA-x	92.5	91.7	89.9		
Crystallinity (%)	A-x	58.3	56.5	56.3	54.5	49.4
	RA-x	56.1	55.6	54.5		
ΔH_c (J/g)	A-x	109.9	105.7	103.2	101.2	96.4
	RA-x	102.8	100.0	98.2		
T_c (°C)	A-x	125.4	126.9	128.8	117.3	110.3
	RA-x	116.4	115.4	114.5		

and 4.24 nm, respectively, showing the increase of 0.82 nm and 1.69 nm compared with Cloisite®20A. In 14 wt % amine-treated clay, there appears a new peak near $2\theta = 4.52°$, which corresponds to the d-spacing of 1.93 nm which may be resulted from the inclusion of HMDA into montmorilonite. The increase of d-spacing was resulted from the intercalation of HMDA into silicate layers. HMDA could be inserted into the silicate layer easily to increase the gallery distance more.

The TGA thermograms of the PP/clay nanocomposites containing 1 wt % inorganic content are shown in Figure 2, and TGA results are summarized in Tables II and III (temperature of 5 wt % weight loss is indicated as T_{95}). Generally, clay particles can improve the thermal stability of polymer by acting as thermal insulator[14] and mass transport barrier[15] to the generated volatile products during decomposition. Similar behavior was observed in the PP/amine-treated clay nanocomposites in this study. The incorporation of the amine-treated clay shows slightly lower thermal stability compared with the one with non–amine-treated Cloisite®20A. The lower thermal stability of A and B series is originated from the free amine group.

Boiling point of HMDA is around 200°C and above this temperature HMDA can be evaporated rapidly which destroys the polymer matrix and causes cracks throughout the surface. This can increase the surface area of the samples where heat can be transferred and weaken the thermal stability. As a matter of fact, the difference of T_{95} between A and RA series (low amine content) is lower than that between B and RB series (high amine content).

DSC heating and cooling thermograms of the PP/clay nanocomposites are shown in Figure 3. The melting temperature (T_m), heat of fusion (ΔH_m), crystallization temperature (T_c), heat of crystallization (ΔH_c), and the degree of crystallinity of the reference sample (PP/PP-g-MA mixture) and the PP nanocomposites were investigated and their results are summarized in Tables IV and V. The percent crystallinity of the nanocomposite was calculated as the ratio of the heat of fusion of the sample to the heat of fusion of the pure crystalline form of PP. The value of pure PP was taken as 165.0 J/g.

The melting temperature of PP nanocomposites measured by DSC shows little change.

The effect of the inorganic content on the crystallization behavior of PP was studied by DSC cooling scans. Usually, the presence of the clay in the nanocomposites increase the crystallization temperature since the clay acts as the nucleating agent. As the amount of the exfoliated clay platelet increases, the number of the available nucleating agent also increases, which will increase the crystallization

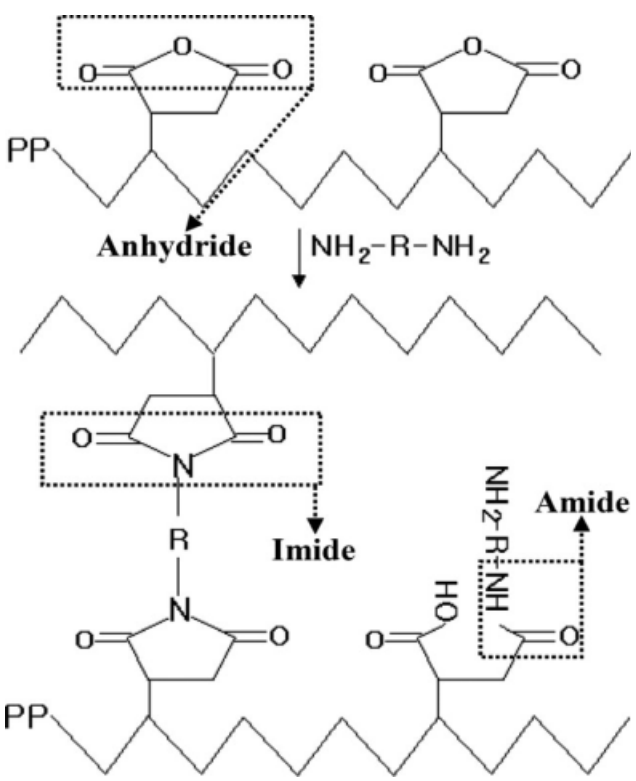

Figure 4 Reaction scheme of amine and MA group.

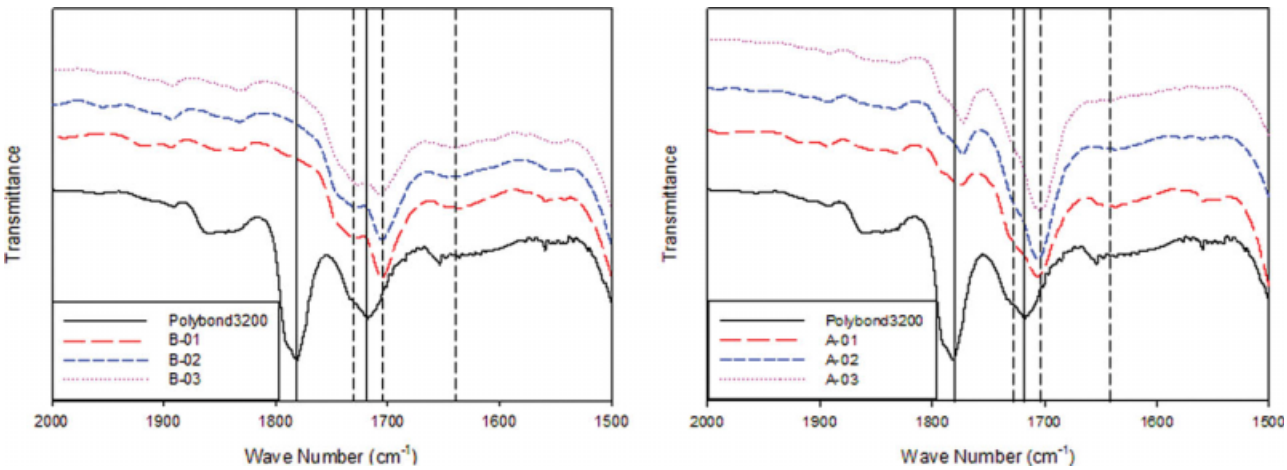

Figure 5 FTIR spectra of HMDA treated-nanocomposite. (a) B-x and (b) A-x. [Color figure can be viewed in the online issue, which is available at www.interscience.wiley.com.]

temperature. In this study, nanocomposites with non–amine-treated clay show little change in T_c, but samples that contain amine-treated clay show higher T_c. ΔH_m, crystallinity, and ΔH_c of amine treated PP nanocomposite also showed higher values than PP nanocomposite with Cloisite20A alone, which indicated better dispersion in amine-treated nanocomposite. This can be the clear evidence that amine groups in clay help silicate layers to disperse well in the polymer matrix. ΔH_m, degree of crystallinity, of 1% amine-treated clay shows higher values than 2 or 3% clay which indirectly indicates better dispersion.

When MA groups reacts with amine group of HMDA, they form either amide or imide linkage as shown in Figure 4. The amide linkage can act as a short chain branching whereas imide linkage act as a long chain branching. In the case of imide linkage, another PP-g-MA chains are attached in the end of nitrogen so that it can form long chain branching. This long chain branching can decrease viscosity of molten sample during the melting process. And this low viscosity helps silicate to be dispersed well in a polymer matrix. In the FTIR spectra (Fig. 5), MA group in PP-g-MA (Polybond3200) shows anhydride and hydrolyzed free acid peak. But when PP-g-MA is reacted with HMDA, the intensity for the absorption peaks of the MA group at 1780 and 1712 cm^{-1} decreased and the absorption at 1702 and 1650 $cm^{-1,}$ which correspond to the carbonyl group of the imide and amide linkage newly appear.[16,17]

In B series, the anhydride peaks at 1780 and 1712 cm^{-1}completely disappeared. But in A series, two peaks did not disappear but they were weakened. Although NH_2 and MA group are in equimolar

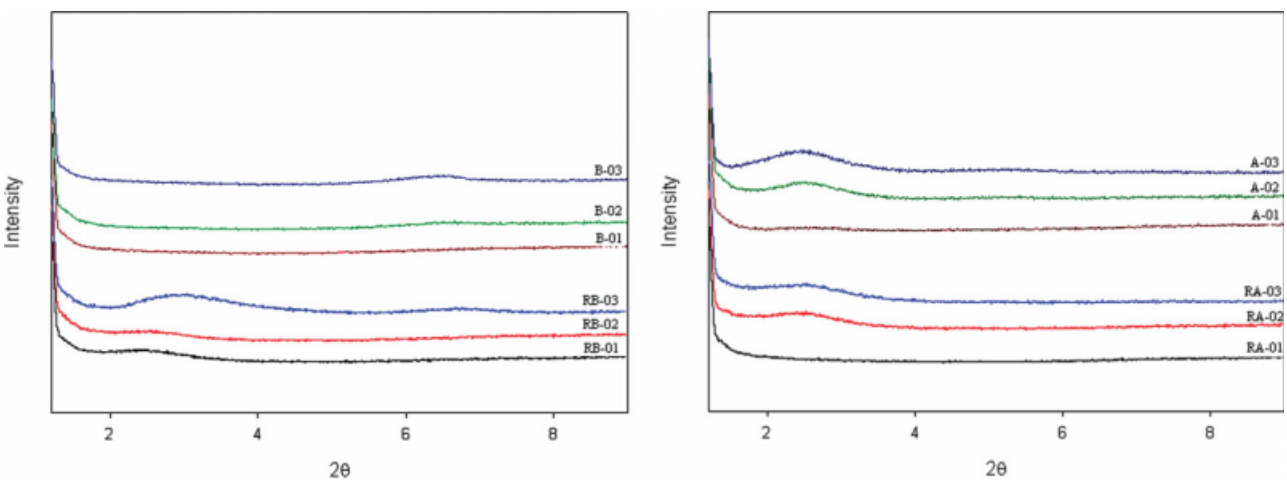

Figure 6 XRD results of nanocomposite (a) nonequimolar composite and (b) equimolar composite. [Color figure can be viewed in the online issue, which is available at www.interscience.wiley.com.]

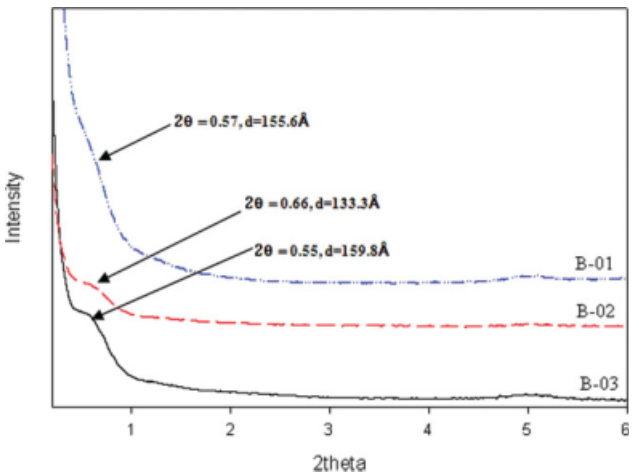

Figure 7 SAX patterns of B series. [Color figure can be viewed in the online issue, which is available at www.interscience.wiley.com.]

composition, the amines inside the gallery (particularly amine not exposed to the surface but in the inner part of the clay clusters) have little chance to react with the anhydride attached to PP-g-MA during the mixing process. To react completely with all the anhydride group in PP-g-MA, the amine/anhydride ratio should be in excess.

Figure 6 shows the WAXD patterns of each sample. The WAXD shows the clay gallery spacing, which indirectly provides information on the degree of dispersion in submicron level. Except B series, all other nanocomposites show intercalated structure from the WAXD results. The absence of the characteristic d_{001} diffraction peak of silicate layers for the B series is the strong evidence for the formation of exfoliated or disordered nanocomposites. In equimolar composite (A series), the amine-treated clays show a little lower peak angle compared with those

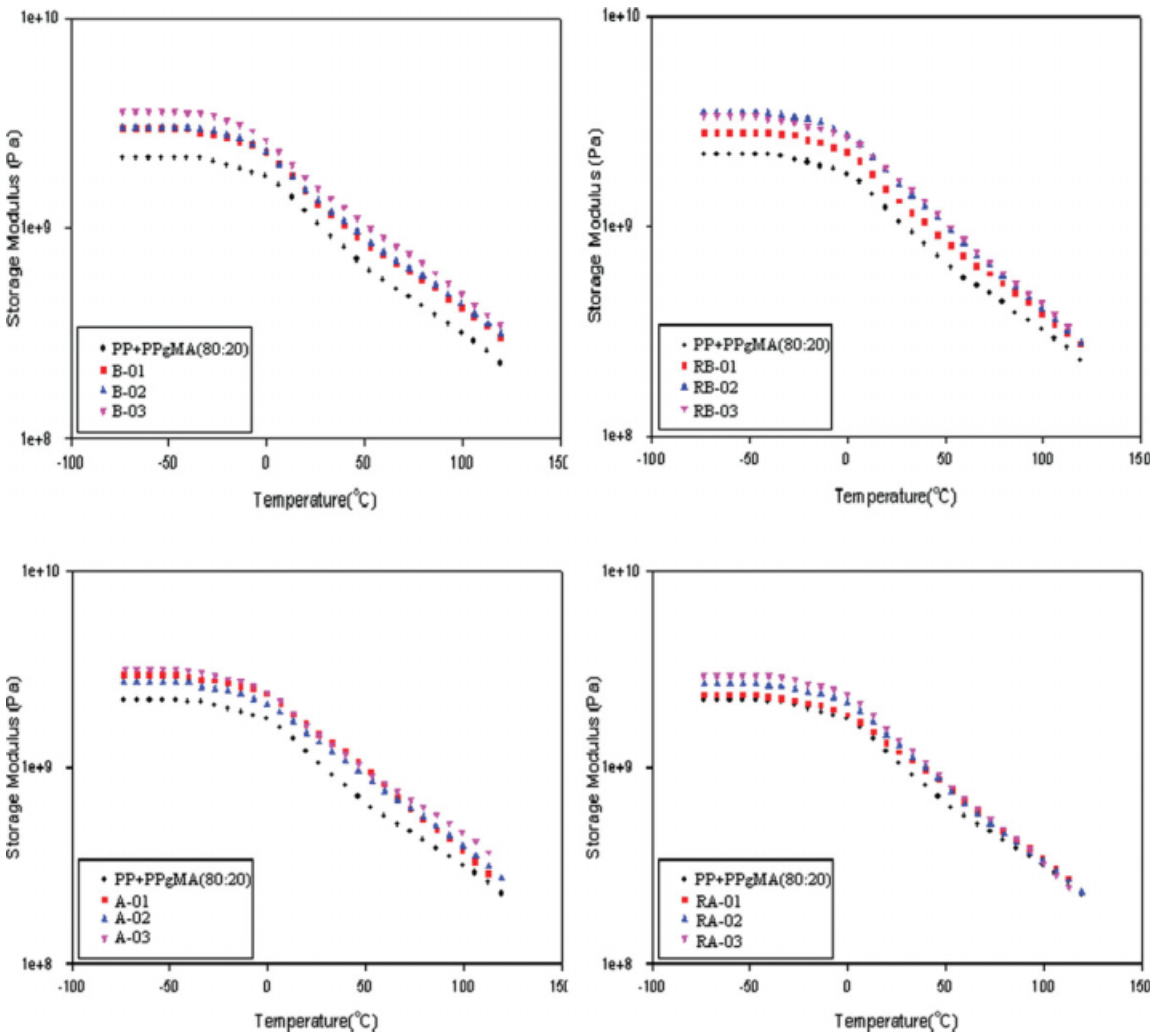

Figure 8 Dynamic storage modulus of nanocomposites (a) B-x, (b) RB-x, (c) A-x, and (d) RA-x. [Color figure can be viewed in the online issue, which is available at www.interscience.wiley.com.]

of non–amine-treated clay. The reaction between the diamines in the organoclay and the anhydride attached in PP chain accelerate the penetration of the PP chain inside the clay gallery. In B series, the effect of amine group is clearly shown, but in A series it is not clear. This result may be explained by the FTIR results. In FTIR results, A series show a clear maleic anhydride absorption peak. It means that they did not react completely with diamine and the penetration of the PP chain inside the silicate gallery is limited.

To investigate the silicate structure of B series clearly, SAXS measurement was conducted. In the WAXD patterns of the nanocomposite, there were no peaks for basal spacing ranging from $2\theta = 1.2^{\circ}$ to 5°. However, the peaks for basal spacing appeared in SAXS patterns as shown in Figure 7. The d-spacings corresponding to $2\theta = 0.55^{\circ}$, 0.66°, and 0.57° were 16.0, 13.3, and 15.6 nm, respectively. So the presence of the exfoliated clay or widely expanded intercalated clay is confirmed.

The dynamic mechanical properties of the PP/clay nanocomposites were measured by DMTA. As shown in Figure 8, the storage modulus (E') increased with increasing clay content. Both B and A series nanocomposites showed higher modulus than RB and RA series. In the case of B-03, the nanocomposites show remarkable increase in stiffness. The improvement of the storage modulus is realized with small amount of clay loading. The improvement originates from the strong interaction between the surface of the dispersed clay and the PP matrix.

The Young's modulus, yield stress, and elongation at break obtained from the tensile measurement are summarized in Figure 9. Young's modulus increased with increasing the clay content. Usually, the insertion of inorganic material to the polymer matrix produces a substantial increase of the modulus. Because clay platelets show high stiffness compared with polymer, the Young's modulus of the nanocomposites are increased.[18] In addition, the formation of amide and imide linkage between MA group and amine group in silicate layer also contributes the enhancement. Young's modulus of the nanocomposites with amine-treated clay shows higher modulus than those of the other nanocomposites. It may result from the interaction of MA and amine group. This interaction could be expected to increase the dispersion of the organoclay in PP matrix. The largest increase in Young's modulus was shown in the case of B-x. Tensile strength shows a decreasing tendency with increasing the clay content. This results from the inevitable aggregation of the clay particles in high clay content.

Usually, Elongation at break decreases with increasing inorganic content. But there is some tendency that B, A series have higher elongation at break than RB and RA series.

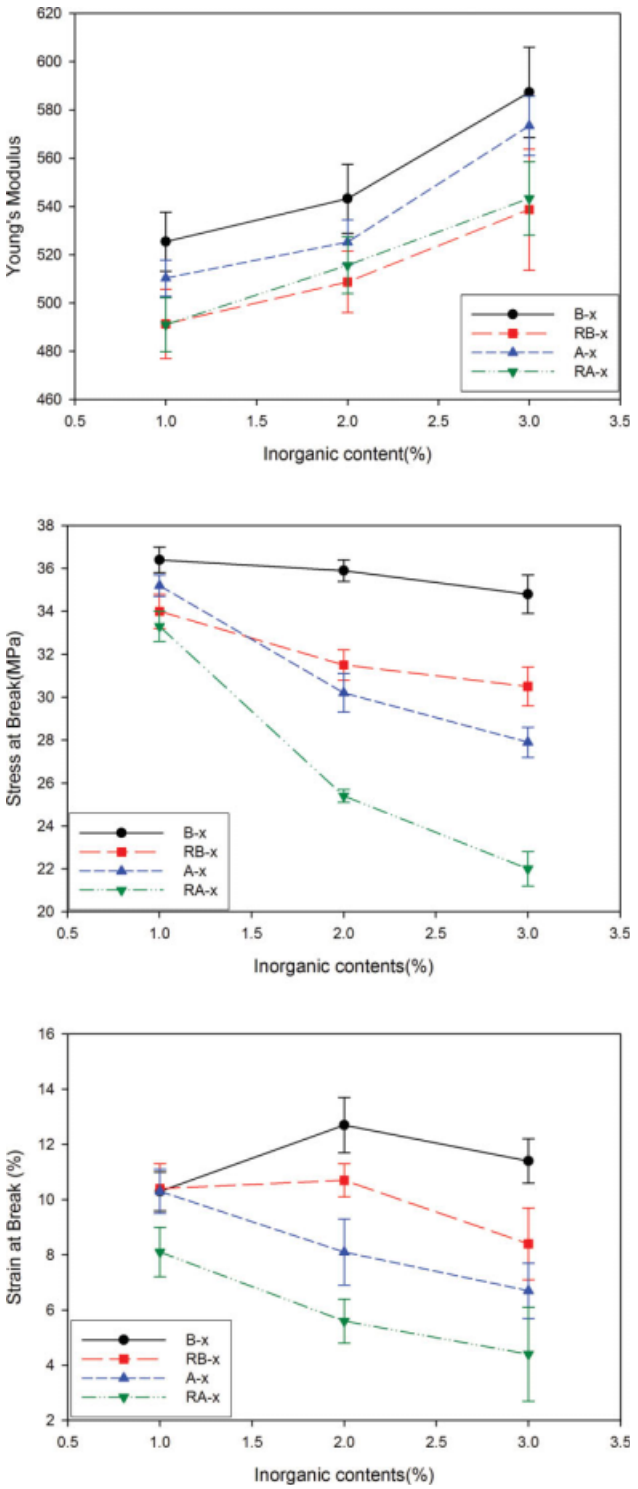

Figure 9 Tensile results of nanocomposites. (a) Young's modulus, (b) stress at break, and (c) strain at break. [Color figure can be viewed in the online issue, which is available at www.interscience.wiley.com.]

Figure 10 shows the SEM micrographs and the particle size distribution of the agglomerated clay particles of the O_2 plasma-etched B-1, RB-1, A-1 and RA-1. The plasma etching of the nanocomposite

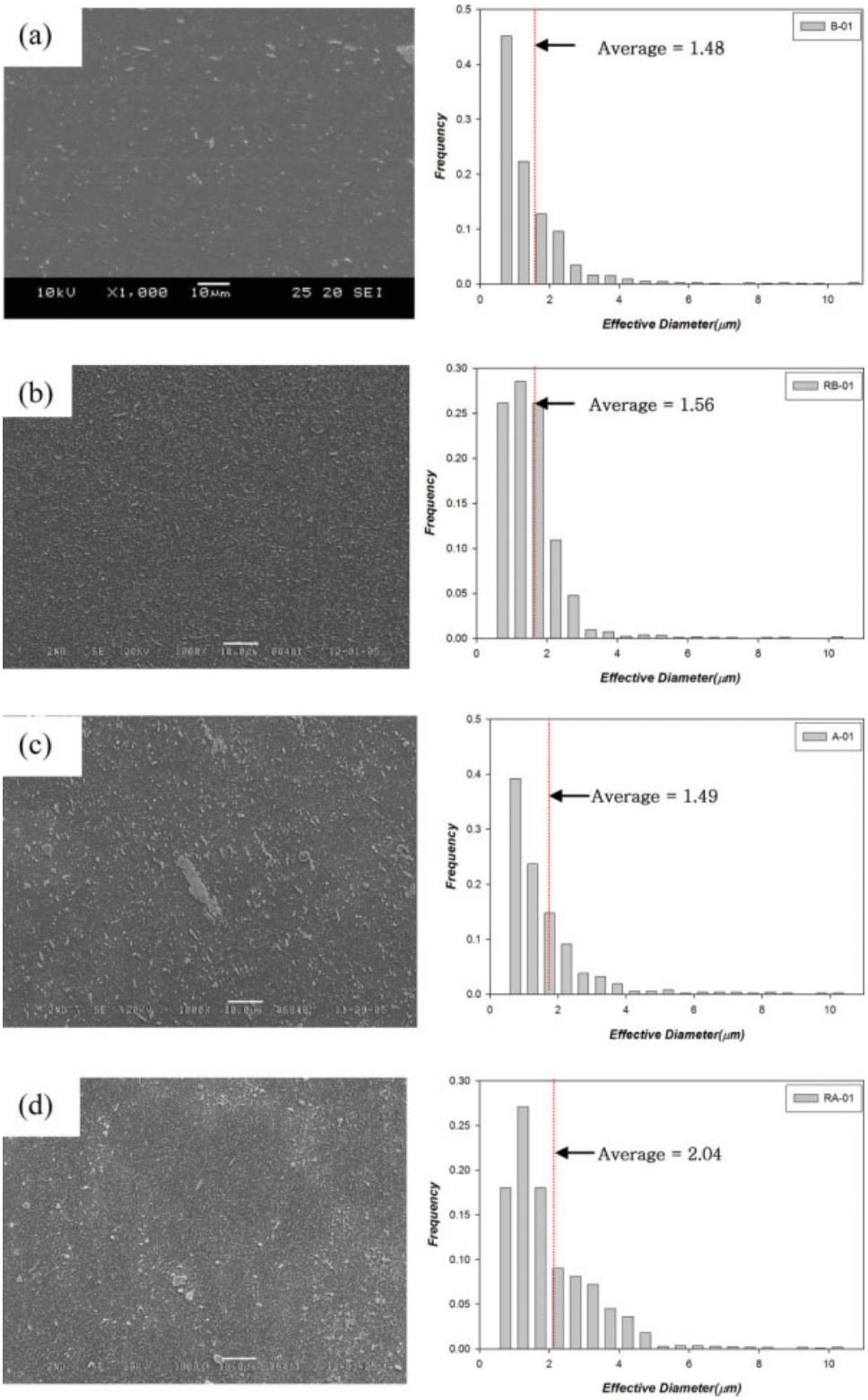

Figure 10 SEM morphology of prepared sample (a) B-01, (b) RB-01, (c) A-01, and (d) RA-01. [Color figure can be viewed in the online issue, which is available at www.interscience.wiley.com.]

surface will expose the residual core particles. The number of residual clay particles increased with the clay loading. Average diameter of the clay particles changed from 1.48 to 3.70 microns. The size of the residual clay particle was smaller when the organoclay had excess diamine and the clay loading was 1%. The residual particle became bigger when the clay was not treated with diamine and the loading

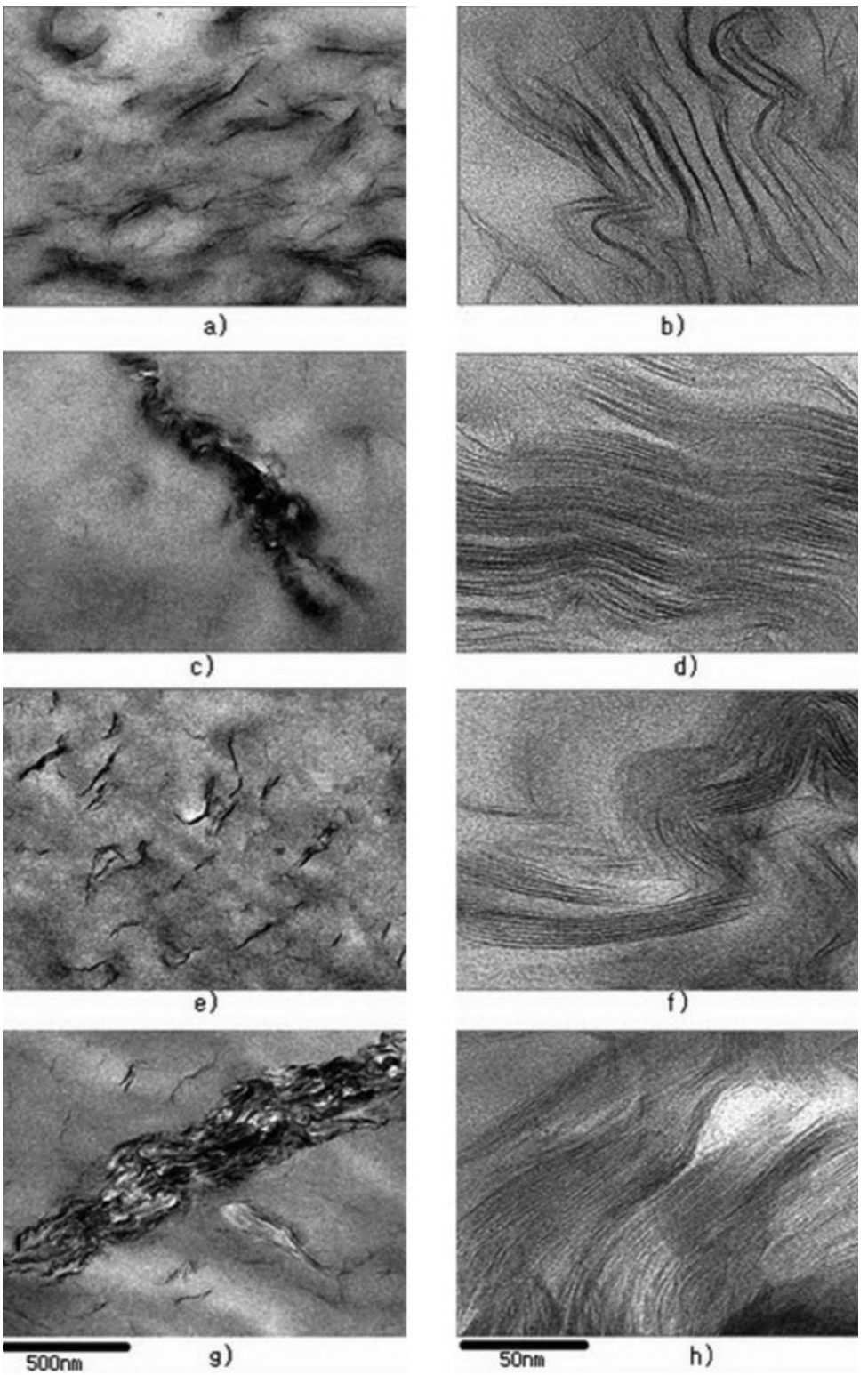

Figure 11 TEM images of the samples. Silicate layers were well dispersed in a continuous matrix (a) low magnification, (b) high magnification of B-02, on the other hand, silicate are agglomerated, (c and d) RB-02, partially intercalated structure, (e and f) A-02, particle in macro scale was found (g and h) RA-02.

was 3%. It seems that the clay particles aggregate more when the clay loading is higher.

TEM micrographs of the PP/clay nanocomposites are shown in Figure 11. In low magnification image, the amine-treated nanocomposites show better dispersibilty compared with those of Cloisite 20A. There was microscale agglomeration of silicate layers in Cloisite 20A. To observe dispersion of silicate

layers more clearly, all the samples was investigated more. In high magnification, silicate layers of amine-treated nanocomposite were exfoliated to individual layers or to some thin stacks containing a few layers while those of Cloisite 20A seem to be shown partial intercalated structure. Compared with Cloisite 20A, amine-treated clays shows a better dispersion irrespective of inorganic contents. Among the samples, B-02, which has noneqimolar ratio between HMDA and MA, had nearly exfoliated structures. And this TEM results coincide well with the SAXS results.

CONCLUSION

In this study, the effect of the insertion of aliphatic diamine in the organoclay on PP nanocomposite was investigated. HMDA that help the dispersion of clay in PP matrix can react with MA groups on polybond3200. New organoclay was prepared through direct insertion of HMDA in molten state using Brabender mixer. From the XRD results, amine group was successfully penetrated into silicate layers. The amount of MA grafted PP was adjusted so that the amine/anhydride ratio varied from 1.0 to 10.4. When the ratio of HMDA was in excess amount (nonequimolar method), the maleic anhydride group reacted completely to form inmide or amide linkage. So the characteristic peak of MA group was not found in FTIR. On the other hand, if the amine and anhydride was in equimolar condition, the MA did not react completely since some amines were not exposed to the surface of the clay cluster and residual anhydride group can be observed in FTIR spectra.

The nanocomposites with amine treated clay, particularly with excess amine (non-equimolar, B-series) showed no peak in WAXD and showed gallery spacing of 13.3 to 16.0nm in SAXS. From the TEM pictures, it is showed that B series have nearly exfoliated structures. In the thermal analysis, well-dispersed clay surfaces provide nucleation site for crystallization. ΔH_m, degree of crystallization and ΔH_c showed maximum at 1% clay loading in B-series, which indicated the better dispersability in 1% clay loading. When the surface of PP nanocomposite was etched by oxygen plasma to reveal the core aggregated clay particle, B-01 showed the least number of core aggregates. The PP nanocomposites with amine-treated clay in nonequimolar method showed the best mechanical performance in Young's modulus, stress at break, and elongation at break. Thus, the insertion of aliphatic diamine in organoclays had significant effect on the degree of dispersion of the clay in PP matrix as well as the enhancement of the mechanical performance of the nanocomposite.

References

1. Kato, M.; Usuki, A.; Okada, A. J Appl Polym Sci 1997, 66, 1781.
2. Kawasumi, M.; Hasegawa, N.; Kato, M.; Usuki, A.; Okada, A. Macromolecules 1997, 30, 6333.
3. Hasegawa, N.; Kawasumi, M.; Kato, M.; Usuki, A.; Okada, A. J Appl Polym Sci 1998, 67, 87.
4. Oya, A.; Kurokawa, Y.; Yasuda, H. J Mater Sci 2000, 35, 1045.
5. Park, M. G.; Venkataramani, S.; Kim, S. C. J Appl Polym Sci 2006, 101, 1711.
6. Choi, W. J.; Kim, S. H.; Kim, Y. J.; Kim, S. C. Polymer 2004, 45, 6045.
7. Wolf, D.; Fuchs, A.; Wagenknecht, U.; Kretzschmar, B.; Jehnichen, D.; Häussler, L. Proceedings of the Eurofiller'99; 1999; p 6.
8. Reichert, P.; Nitz, H.; Klinke, S.; Brandsch, R.; Thomann, R.; Mülhaupt, R. Macromol Mater Eng 2000, 275, 8.
9. Manias, E.; Touny, A.; Wu, L.; Lu, B.; Strawhecker, K.; Gilman, J. W.; Chung, T. C. Polym Mater Sci Eng 2000, 82, 282.
10. Manias, E.; Touny, A.; Wu, L.; Lu, B.; Chung, T. C. Macromolecules, to appear.
11. Usuki, A.; Kojima, Y.; Kawasumi, M.; Okada, A.; Fukushima, Y.; Kurauchi, T.; Kamigaito, O. J Mater Res 1993, 8, 1179.
12. Reichert, P.; Nitz, H.; Klinke, S.; Brandsch, R.; Thomann, R.; Mülhaupt, R. Macromol Master Eng 2000, 375, 8.
13. Kim, K. Y.; Kim, S. C. Int Polym Process 2004, 19, 356.
14. Zanetti, M.; Camino, G.; Thomann, R.; Mülhaupt, R. Polymer 2001, 42, 4501.
15. Wang, Z.; Pinnavaia, T. J. Chem Mater 1998, 10, 3769.
16. Tseng, F. P.; Lin, J. J.; Tseng, C. R.; Chang, F. C. Polymer 2001, 42, 713.
17. Song, Z.; Baker, W. E. J Polym Sci: Part A: Polym Chem 1992, 30, 1589.
18. Noh, M. H.; Jang, L. W.; Lee, D. C. J Appl Polym Sci 1994, 74, 179.